Combining land surface models and remote sensing data to estimate evapotranspiration for drought monitoring in Europe

C. Cammalleri*[a], G. Sepulcre-Cantó[b], J. Vogt[a]
[a] European Commission, Joint Research Centre (JRC), 21027 Ispra (VA), Italy; [b] Catholic University of Louvain, Earth and Life Institute, B-1348 Louvain-la-Neuve, Belgium.

ABSTRACT

The main hydrologic feedback from the land-surface to the atmosphere is the evapotranspiration, ET, which embraces the response of both the soil and vegetated surface to the atmospheric forcing (e.g., precipitation and temperature), as well as influences locally atmospheric humidity, cloud formation and precipitation, the main driver for drought. Actual ET is regulated by several factors, including biological quantities (e.g., rooting depth, leaf area, fraction of absorbed photosynthetically active radiation) and soil water status. The ET temporal dynamic is strongly affected by rainfall deficits, and in turn it represents a robust proxy of the effects of water shortage on plants. These characteristics make ET a promising quantity for monitoring environmental drought, defined as a shortage of water availability that reduces the ecosystem productivity.

In the last few decades, the capability to accurately model ET over large areas in a spatial-distributed fashion has increased notably. Most of the improvements in this field are related to the increasing availability of remote sensing data, and the achievements in modelling of ET-related quantities. Several land-surface models exploit the richness of newly available datasets, including the Community Land Model (CLM) and the Meteosat Second Generation (MSG) ET outputs.

Here, the potentiality of ET maps obtained by combining land-surface models and remote sensing data through these two schemes is explored, with a special focus on the reliability of ET (and derived standardized variables) as drought indicator. Tests were performed over Europe at moderate spatial resolution (3-5 km), with the final goal to improve the estimation of soil water status as a contribution to the European Drought Observatory (EDO, http://edo.jrc.ec.europa.eu).

Keywords: Community land model, Meteosat second generation, soil-vegetation-atmosphere transfer.

1. INTRODUCTION

Evapotranspiration, ET, representing the total of the water losses from the surface to the atmosphere, through evaporation and transpiration, can be seen as a key parameter for water stress assessment over vegetated areas. ET process is controlled by both external meteorological forcing and soil water availability. When water availability becomes a limiting factor, plants react by reducing the transpiration fluxes with respect to the atmospheric demand (namely ET_o). It is clear that the ratio between the former (ET) and the latter (ET_o) represents a direct indicator of vegetation water stress, useful to quantify the occurrence of water deficit conditions.

The actual ET is a main component of both surface water and energy balances, this justifies the use of either hydrological models[1,2] or residual surface energy balance approaches[3,4] for its spatially distributed estimation. The first exploit the availability of rainfall inputs to model soil moisture dynamics, whereas the second use the land-surface temperature observed from satellite as proxy of the land water status.

The more sophisticated land-surface models are able to jointly solve the water-energy budget, as well as most of the other main land-atmosphere exchange processes[5] (i.e., carbon and nitrogen). These models take full advantage of the accessibility of spatially distributed information related to land properties (e.g., land cover, vegetation traits) thanks to the increasing availability of remotely sensed satellite data.

*carmelo.cammalleri@jrc.ec.europa.eu; phone +39 0332-78-9869; http://edo.jrc.ec.europa.eu

For moderate-to-low spatial resolution applications (from 1 to 100 km) land-surface models developed a variety of mosaicking systems to reproduce the within-pixel heterogeneity of the landscape that is commonly observed in the real world. Among the most common land-surface models, we identified two approaches that seem suitable for a near-real time monitoring of ET for drought applications at moderate spatial resolution (5-km) over the European domain: 1) the Community Land Model (CLM[6]), and 2) the Meteosat Second generation (MSG) ET product (MET[7]) developed by the Land Surface Analysis Satellite Application facilities (LSA-SAF, http://landsaf.meteo.pt/).

The CLM approach is the land-surface component of the coupled climate Community Earth System Model (CESM), designed to simulate the exchange processes of water, energy and momentum between soil, vegetation and atmosphere, constituting one of the most complete modelling of the land-atmosphere interactions. The land-surface is schematized as nested grids representing different land units (glacier, lake, wetland, urban, vegetation). The vegetated surfaces are represented as a composition of plant functional types (PFTs). The model reproduces the main hydrological processes, including interception, canopy drip, infiltration, evaporation, surface runoff, plant uptake and transpiration, sub-surface drainage and groundwater storage.

The MET product is based on a simplified soil-vegetation-atmosphere scheme modified to accept inputs from external sources[8]. This method is based on the physics of the Tiled ECMWF Surface Scheme for exchange processes over land (TESSEL[9]), as well as on an extensive use of LSA-SAF operational products. The land-surface in each pixel is represented with up to six tiles over land (bare ground, low and high vegetation, intercepted water, and shaded and exposed snow) and two over water (open and frozen water), with separate energy and water balances. The model fully solves the surface energy budget using as further inputs the soil moisture and temperature profiles provided by TESSEL. The MET maps are made available operationally over the whole European continent, as well as over Africa, at MSG spatial resolution (about 5-km) every 30 min. MET products were specifically designed for a routine monitoring of ET at regional to continental scale.

In this paper the potential use of ET maps modelled by CLM and MET land-surface approaches to detect water stress conditions is explored, focusing on the capability to capture both ET dynamics and water deficit magnitude. The analysis is part of testing the suitability of such products for drought monitoring within the framework of the European Drought Observatory (EDO, http://edo.jrc.ec.europa.eu). With this aim, the results of the two models were inter-compared, as well as validated against in-situ data collected with flux towers. Special attentions was given to the capability to detect water stress conditions during the conventional growing season for Europe (April to September).

2. DESCRIPTION OF THE MODELS

2.1 CLM model

The Community Land Model (CLM) fully simulates the exchanges of gasses, water, energy and momentum between land surface and lower atmosphere (Fig. 1). The model version 4.0 was adopted in this study, released within CESM 1.0.5. Different configurations (namely "component-sets" or *compsets*) of the model can be run on the base of the "active" components. In particular, in this study the I-*compset* was used, in which only the land component is active, whereas the atmosphere component is in data mode (external inputs) and the other components (ocean, ice and glacier) are stub. Within I-*compset*, it is possible to choose between the SP (Satellite Phenology) and the CN (Carbon-Nitrogen biogeochemistry) versions. In the adopted I-SP *compset*, both atmospheric forcing and plant phenology are directly provided as model inputs.

As already mentioned, the model reproduces all the main biogeo -physical and - chemical processes that occur at the interface between low atmosphere and land-surface, including: water, energy and momentum fluxes, exchange of trace gasses and particle (e.g., Carbon, Nitrogen, dust). The budgets are solved at cell scale, with each cell constituted by nested grids representing different land units (glacier, lake, wetland, urban, vegetation). The vegetated surfaces are represented as a composition of up to 15 plant functional types (PFTs) plus a bare soil. All the PFTs share the same soil column, which is modelled by means of 10 hydraulically active (and 5 inactive) layers vertically distributed according to an exponential law. Since our main goal is to test the reliability of the modelled ET for drought monitoring, in the next section we will focus on the water (hydrological) balance component of the model, with particular attention to the effects of water deficit on actual ET.

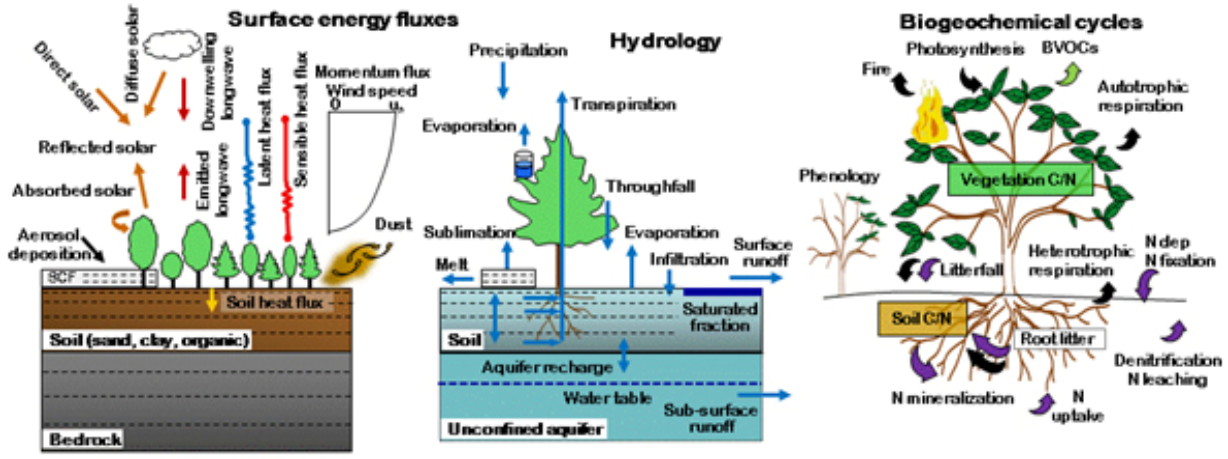

Figure 1. Schematization of the main land-surface balances resolved by CLM: energy (left panel), water (center panel), and carbon/nitrogen (right panel) (http://www.cesm.ucar.edu/models/clm/).

The relationship among the main hydrological processes that occur in the soil-vegetation-atmosphere continuum is represented in CLM through the surface water budget, defined as:

$$\Delta W_c + \Delta W_s + \sum_{j=1}^{N}\left(\Delta w_{w,j} + \Delta w_{i,j}\right) + \Delta W_a = \left(Q_r + Q_s - E_c - E_g - Q_o - Q_d - Q_{rs}\right)\Delta t \qquad (1)$$

where ΔW_c, ΔW_s and ΔW_a are the variations in canopy, snow and aquifer water, respectively, $\Delta w_{w,j}$ and $\Delta w_{i,j}$ are the changes in soil liquid and ice water at the j-th layer (out of N soil layers), respectively, Q_r is the rainfall, Q_s is the solid precipitation, E_c is the canopy evapotranspiration, E_g is the soil evaporation, Q_o is the surface runoff, Q_d is the sub-surface drainage and Q_{rs} includes the runoff from other surfaces (glaciers, wetlands, lakes) and Δt is the time step (s). All the left-hand terms are in (kg m^{-2}), whereas the right-hand terms are in (kg m^{-2} s^{-1}).

The total evapotranspiration, $E = E_c + E_g$, is modelled as part of the surface energy budget following the Monin-Obukhov similarity theory developed for the surface layer. For vegetated surfaces, these fluxes can be defined as:

$$E = -\rho\frac{q_a - q_s}{r_{aw}} = E_c + E_g = -\rho\left(\frac{q_s - q_c}{r_{\mathrm{tot}}} + \beta_s\frac{q_s - q_g}{r'_{aw}}\right) \qquad (2)$$

where ρ s the air density (kg m^{-3}), q_a is the atmospheric specific humidity (kg kg^{-1}), q_s is the surface specific humidity (kg kg^{-1}), r_{aw} is the aerodynamic resistance to water vapor transfer (s m^{-1}), q_c is the specific humidity in the canopy air space (kg kg^{-1}), q_g is the specific humidity at ground level (kg kg^{-1}), r_{tot} is the total resistance to water vapor transfer from canopy (s m^{-1}), including contributes from leaf boundary layer and stomatal resistance (r_s), r'_{aw} is the aerodynamic resistance to water vapor transfer between ground and canopy air space (s m^{-1}), and β_s is an empirical function to account for the effects of soil water content on soil evaporation.

The stomatal control on canopy transpiration (as well as on carbon assimilation) is simulated through the Ball-Berry conductance model as described by Collatz et al.[10]. This model relates stomatal conductance (i.e., the inverse of resistance) to net leaf photosynthesis, scaled by the relative humidity at the leaf surface and the CO_2:

$$\frac{1}{r_s} = m\frac{A}{c_s}\frac{q_s}{q_c}P_{\mathrm{atm}} + b \qquad (3)$$

where m is a PFT-depended parameter, A is the net leaf photosynthesis (μmol CO_2 m^{-2} s^{-1}), c_s is the CO_2 partial pressure at the surface level (Pa), P_{atm} is the atmospheric pressure (Pa), and b = 2000 is the minimum stomatal conductance when $A = 0$. Typical values are: $m = 9$ for C3 plants and $m = 4$ for C4 plants[11,12].

Leaf photosynthesis is computed based on the model of Farquhar et al.[13] for C3 plants and Collatz et al.[11] for C4 plants. In both cases, A can be seen as a function of the maximum rate of carboxylation (V_{max}); the latter is derived from canopy leaf temperature, T_c, and a soil water function β_t, which accounts for the effects of water deficit on stomata closure. This function is computed as a weighted average of soil water potential in the root zone:

$$\beta_t = \sum_{j=1}^{N} r_j w_j \tag{4}$$

where w_j is the plant wilting factor in the j-th soil layer and r_j is the fraction of roots in the same layer. The plant wilting factor is computed from the soil water matric potential, ψ_j (mm), as:

$$w_j = \frac{\psi_c - \psi_j}{\psi_c - \psi_o} \tag{5}$$

where ψ_c and ψ_o are the soil water potential (mm) when stomata are fully closed or fully open, respectively.

2.2 MET model

The evapotranspiration algorithm developed in the framework of LSA-SAF (MET) focuses on quantifying both canopy and soil water fluxes to the atmosphere using input data derived from MSG geostationary satellite. The adopted methodology can be described as a soil-vegetation-atmosphere transfer (SVAT) scheme decoupled from the atmospheric model and forced by radiation inputs derived from MSG data and soil variables (temperature, water content) derived from ECMWF forecasts. Similarly to CLM, the elementary spatial unit of the model (pixel) is constituted by a composition of different vegetation/non-vegetation primary types, called tiles. For each pixel, a maximum of three tiles (plus a bare soil) is allowed. At tile level, the surface energy budget is solved, as:

$$R_{n,i} - H_i - \lambda ET_i - G_i = 0 \tag{6}$$

where the subscript i represent the tile, R_n is the net radiation, H is the sensible heat flux, λET is the latent heat flux and G is the heat conduction flux into the ground (all the fluxes are expressed in W m^{-2}); the modelled fluxes are aggregated at pixel scale using the land cover fraction of each tile type.

Net radiation computation is forced by incoming solar radiation, long-wave radiation and surface albedo maps derived from MSG data. Heat flux conducted into the ground is computed as a simple function of R_n and leaf area index (LAI)[14]. Turbulent fluxes are computed via a resistance approach as:

$$H_i = \rho c_p \frac{T_{sk,i} - T_a}{r_{a,i}} \tag{7}$$

$$\lambda ET_i = \lambda \rho \frac{q_s - q_a}{r_a + r_c} \tag{8}$$

where c_p is the specific heat capacity of air (J kg^{-1} K^{-1}), $T_{sk,i}$ is the skin layer temperature (K), T_a is the air temperature (K), r_a is the aerodynamic resistance (s m^{-1}), λ is the latent heat of vaporization (MJ kg^{-1}), and r_c is stomata resistance (s m^{-1}). All other variables as defined in Eq. (2). It is clear how the term r_c in eq. (8) is analogous to the term r_s in Eq. (3); however, in MET the formulation adopted to compute r_c is the one proposed by Jarvis[15] (rather than the Ball-Berry model):

$$r_c = \frac{r_{\min}}{LAI} f_1 f_2 f_3 \tag{9}$$

where r_{min} is a vegetation-specific minimum stomatal resistance (s m^{-1}), f_1 is a radiation stress function, f_2 is a soil water content stress function and f_3 is an atmospheric water pressure deficit stress function. The water stress function f_2 is analogous to the plant wilting factor reported in Eq. (5), even if it is computed on root zone average soil water content (θ) rather than matric potential. The leaf area index (LAI) is used to upscale the resistance from leaf to plant scale.

The system of Eqs. (6)-(8) is solved for H, λET and T_{sk} through an iterative method, due to the non-linear interdependence of the unknown variables into the solving system. The effects of soil water deficit into the energy balance is accounted via the soil moisture and temperature profiles modelled by the TESSEL algorithm at 4 soil layers.

3. STUDY AREA AND MATERIALS

Models' intercomparison was performed over Europe for the year 2011. The CLM model was run from 1997 to 2012 on a lat/lon regular grid domain with a spatial resolution of about 0.05 degree. The model was run at 1 hour time steps and the data were temporarily aggregated to daily scale. The MET data were downloaded from LSA-SAF for 2011; the approach produces ET maps at the MSG spatial resolution (about 4 × 5 km^2 over Europe) every 30-min as well as a daily average. Daily ET maps for both models were resampled on a 5-km regular grid in GISCO Lambert Azimuthal Equal Area projection. The data were also aggregated at monthly scale as a simple average of the daily values for each month.

In the next sub-sections a brief description of the main inputs of each model is provided, as well as an overview of the in-situ data used for the validation of the model outputs.

3.1 Input data for the land-surface models

Given that both CLM and MSG are, up to a certain extent, similar land-surface models, some common features in the required inputs can be identified. The main model inputs can be roughly subdivided into three categories: 1) land coverage and vegetation properties; 2) soil properties (optical, thermal, hydraulic); and 3) meteorological forcing. The data reported in Table 1 summarize the inputs used for each model.

In CLM, climatological LAI monthly maps for each PFT were derived from the Moderate Resolution Imaging Spectroradiometer (MODIS) data collected in 2001-2003; the data were processed at 0.05 degree resolution and successively aggregate at 0.5 degree[16]. Land coverage data were derived from a mixture of sources, most notably PFT sources include Advanced Very High Resolution Radiometer (AVHRR) and MODIS continuous fields, urban areas were derived from the LandScan population density dataset and glaciers from the International Geosphere-Biosphere Programme (IGBP) DISCover dataset[17].

Table 1. List of the main input variables of CLM and MET approaches and corresponding data sources.

VARIABLE	CLM	MET
LAI	MCD15A2 (2001-2003)	ECOCLIMAP
LAND COVER	IGBP DISCover + LandScan + AVHRR/MODIS (1993-2001)	
SOIL PROPERTIES	IGBP	N/R
SOIL MOISTURE	Modelled (10 layers)	TESSEL (4 layers)
SOIL TEMPERATURE		
ALBEDO	Modelled + Soil color from MODIS	LSA-SAF AL product
SOLAR RADIATION	ERA-Interim + MeteoConsult	LSA-SAF DSSF product
LONG-WAVE RADIATION		LSA-SAF DSLF product
METEOROLOGICAL FORCING		ECMWF forecasts

On the other hand, MET surface parameters are derived from the ECOCLIMAP dataset[18], developed by Meteo-France at 1-km resolution specifically for SVAT schemes. In ECOCLIMAP, AVHRR data from 1992 to 1993 (and 1997 only for Europe) were used to retrieve a climatological monthly LAI and the CORINE land cover classification was preferred over Europe to define tile types.

Soil properties are treated quite distinguishably by the two models; CLM, as full land-surface scheme, simulates both soil moisture and temperature profiles starting from soil properties derived from soil texture and organic content maps. The latters were obtained from the IGBP dataset at 0.083 degree[19,20]. MET, instead, does not solve the soil water and thermal budgets, but it uses the outputs of TESSEL model as input; for this reason MET does not require any information on soil properties as direct inputs. Soil optical properties (i.e., albedo) are modelled in CLM separately for vegetated and soil units starting from standard values (for dry and wet canopy and for different classes of soil color derived from MODIS) and introducing the effects of water content. Differently, MET takes advantage from the albedo product provided by LSA-SAF at the MSG spatial resolution (AL)[21].

CLM standard meteorological forcing for version 4.0 is the one provided by Qian et al.[22] at the T42 spatial resolution (~2.8° longitude by 2.8° latitude) from 1948 to 2004. However, for this specific study a high spatial resolution dataset (at 5-km) was extracted from the JRC MARS and the EU-FLOOD-GIS databases[23]. MET meteorological forcing can be subdivided into two classes: i) radiative variables and ii) numerical weather prediction data. The maps from the first class are directly derived from LSA-SAF products for downward surface short-wave flux (DSSF)[24] and downward surface long-wave flux (DSLF)[25], whereas the variables in the second group are retrieved from ECMWF forecasts and spatially interpolated over the MSG grid.

3.2 In-situ evapotranspiration fluxes

The daily ET maps produced by the two models were evaluated against in-situ measurements collected by Fluxnet stations (http://fluxnet.ornl.gov/). Fluxnet is a coordination of different regional micrometeorological networks, mainly focused on the monitoring of the exchanges of carbon dioxide, water vapor, and energy between terrestrial ecosystems and the atmosphere. Half-hourly records of the four main energy fluxes (R_n, G, λET and H) where collected by several stations; however, only 14 sites have provided robust datasets for 2011, these sites are reported in Fig. 2.

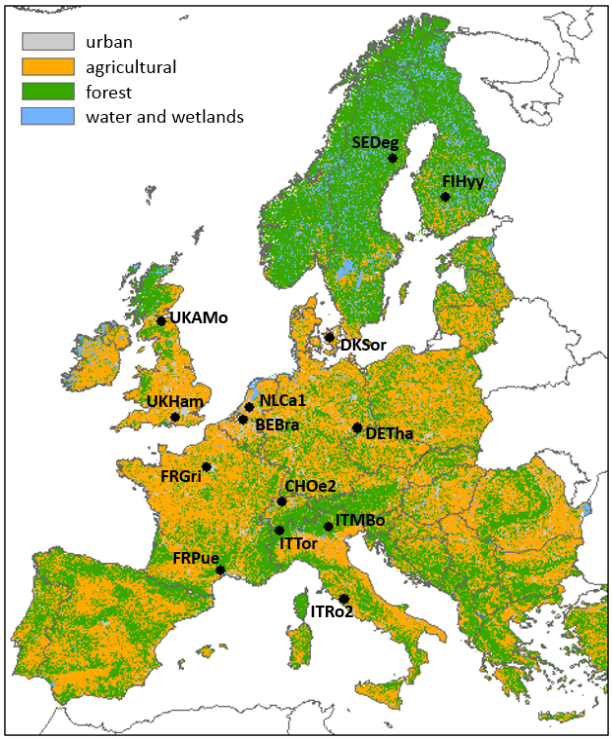

Figure 2. Location of the Fluxnet sites adopted in this study. Fluxnet sites are superimposed on the CORINE land-use map.

Most of the collected datasets do not disseminate heat conduction fluxes into the ground, for this reason it was neither possible to check energy balance closure of the observed data nor to force the closure following one of the methodologies commonly adopted in the literature[26]. Given that closure errors between 10 and 30% are commonly considered acceptable in the literature and soil heat flux is about 10% of R_n[27], from the full dataset the data for which the ratio $(\lambda ET+H)/R_n$ during daytime was smaller than 0.5 were also removed.

Daily ET fluxes were obtained by a simple sum of the half-hourly data, only for that dates with a full daily dataset available (48 observations). Monthly average values were also obtained by averaging all the available daily observations for a given month (with at least 10 days).

4. RESULTS AND DISCUSSION

The analysis of the ET maps produced by the two models was performed following two steps: i) a preliminary intercomparison of the outputs of CLM and MET was performed on the whole domain, mainly focusing on monthly data; ii) an evaluation against in-situ data was performed at local scales using the Fluxnet data as ground truth.

4.1 Intercomparison of CLM and MET models

As first look of the dynamics of the modeled ET, the maps in Fig. 3 show the standardized monthly ET simulated by MET and CLM models. The ET values are standardized using the year average and standard deviation in order to remove eventual biases (analyzed successively).

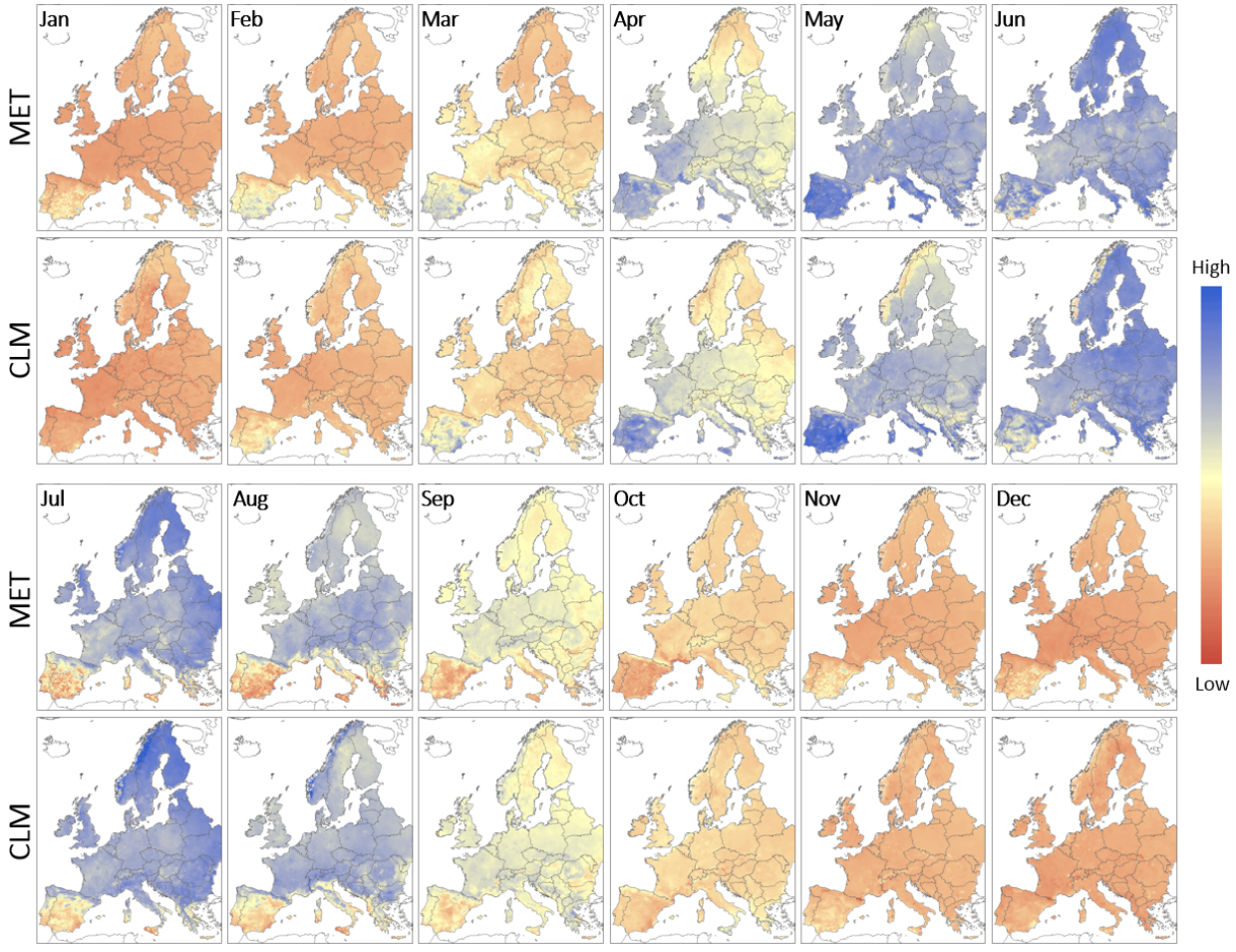

Figure 3. Maps of monthly average standardized ET simulated by MET (first and third lines) and CLM (second and forth lines) over Europe for 2011. Data are standardized by mean of the year average and standard deviation.

These maps show a substantial agreement in the temporal dynamic simulated by the two models, mainly due to the similar seasonality of ET forced by the solar yearly cycle. Also the spatial distribution of standardized ET looks similar for most of the months all-over the domain; some notable exceptions are seen over the Iberia Peninsula during December and January and in Scandinavia during May-June.

The qualitative results observed in the previous maps are confirmed by the unbiased Mean Absolute Difference (ubMAD[28]) maps reported in Fig. 4. These differences, expressed as a multiple of the year standard deviation, show high values over the Iberia Peninsula for most of the months and substantially negligible differences over central Europe. Far East countries show some discrepancies mainly from April to June, and in the same months high ubMAD values are observed also over the Scandinavian Peninsula. Other Mediterranean countries, such us Italy and Greece, display behavior similar to Iberia peninsula during warm months (April to September) but less marked differences during winter months (i.e., November to February).

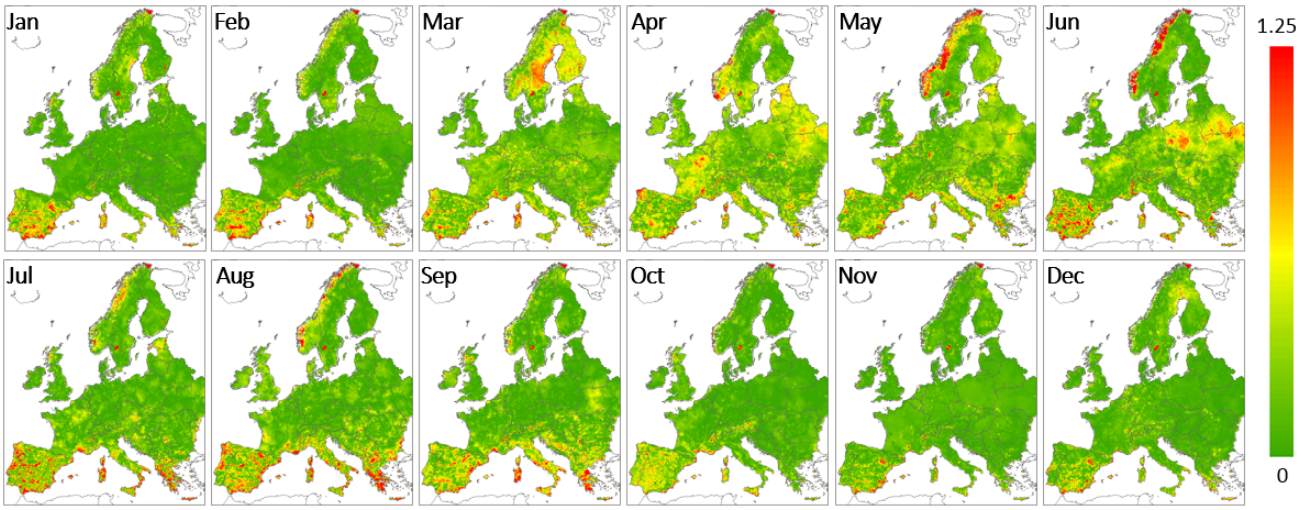

Figure 4. Maps of monthly unbiased Mean Absolute Difference (ubMAD) expressed in multiple of year standard deviation.

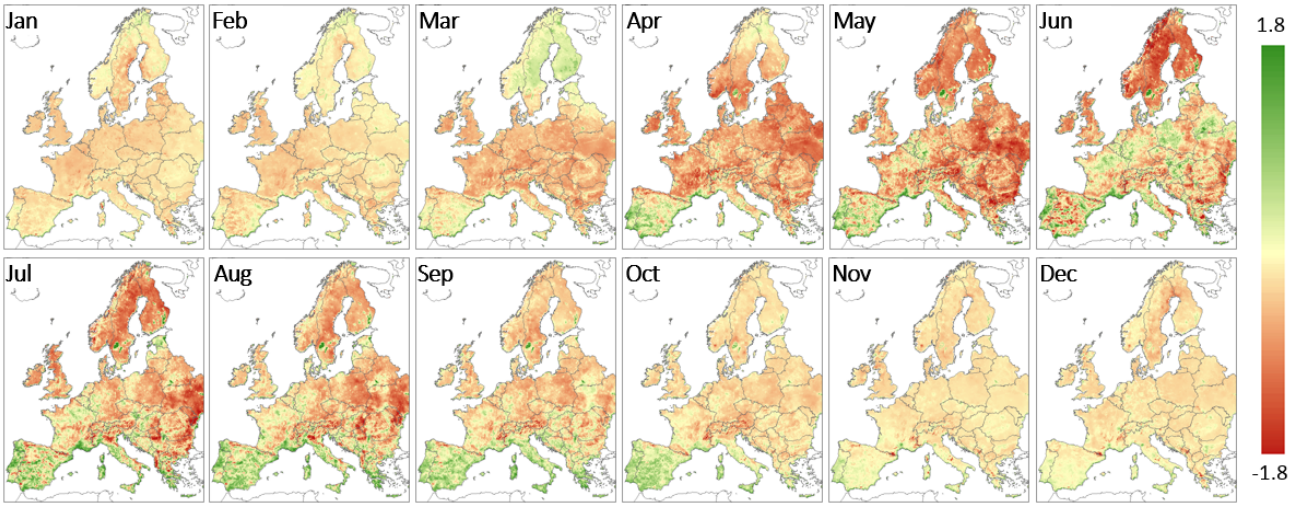

Figure 5. Maps of monthly ET Bias (CLM − MET) expressed in mm d^{-1}.

A complementary information is represented by the bias (computed as the difference between CLM and MET) monthly maps reported in Fig. 5. These maps highlight that even if the two models show similar temporal dynamics, relevant differences can be observed in the magnitude of the simulated fluxes, especially when ET reaches the highest values (approximately from May to August). The two models seem quite close (no bias) from November to February, whereas MET tends to "overestimate" ET compared to CLM during most of the growing period, except for Spain and some other Mediterranean regions where CLM shows higher ET values than MET. The word overestimation is here used as relative term only, since no information on the "true" state are available at this point. During the peak months of ET, the bias can reach quite high values (> 1.5 mm d^{-1}) over large areas; however, these biases may be not a relevant issue for drought detection if they are systematic, since normalization procedures are commonly developed to derive drought indicators from ET (i.e., anomalies).

Following the latter point, an analysis of the correlation between MET and CLM ET maps was performed in order to highlight the analogies in the simulated dynamics. Given that drought detection is often based on water stress indices rather than actual ET, the analysis was performed on both ET and the ratio between ET and the reference evapotranspiration (ETo). The latter was derived from the FOODSEC Meteodata distribution Page (http://marswiki.jrc.ec.europa.eu/datadownload/index.php) as 1-day aggregated maps at 0.25° spatial resolution; the data were resampled to 5-km resolution using the nearest neighbored method.

The correlation was performed on the data collected between April and September, correspondingly approximately to the "standard" growing season for most of Europe. This allow us to avoid issues related to the use of the ratio ET/ETo during the dormant (non-vegetated) period. The maps of the Pearson coefficient computed over the ET and the ET/ETo datasets are reported in Fig. 6 (left and right panels, respectively).

The map in Fig. 6 (left panel) highlights the high correlation observed between the two ET datasets during the growing season over most of the European domain. With the exception of a large agricultural area in the north of France, almost all the domain is characterized by *r* values greater than 0.85. The north of France was affected in spring 2011 by a meteorological drought due to considerably less precipitation occurred in that period compared to the climatology[29]. This likely causes a rapid reduction in ET, due to the reduction in soil water availability, which may be captured differently by the two models. An in deep analysis of this area is performed in the next section.

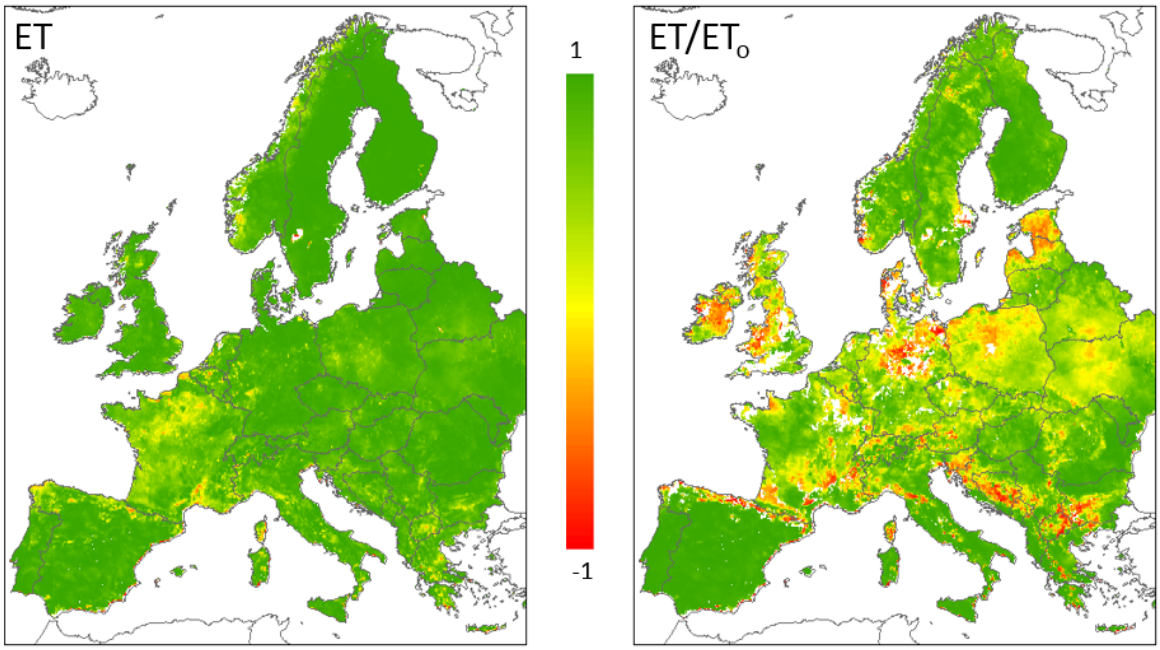

Figure 6. Maps of the Pearson correlation coefficient (*r*) computed between MET and CLM using the data simulated between April and September 2011. The map on the left shows the *r* values obtained for ET whereas the map on the right shows the *r* values obtained for the water stress index ET/ETo.

The overall high *r* values observed for ET may be partially explained by the obvious similar seasonality observed in both ET datasets (see Fig. 3); for this reason, the normalization performed through ETo represents an important test on the agreement in the dynamics simulated by the two models. The correlation map reported in Fig. 6 (right panel) confirms that the *r* values decrease if ET/ETo is analyzed rather than ET, with exceptions over most of the Mediterranean and the Scandinavia. The former is commonly characterized by a large dynamic in the water availability (of which ET/ETo is a proxy) that is similarly modelled by the two approaches, even if the magnitude of the ET fluxes are quite different (see bias maps in Fig. 5); the latter is instead characterized by a peculiar solar radiation yearly cycle due to the high latitude.

Part of the areas with lower *r* values (or even negative ones) are located over impervious terrains, see for instance: Pyrenees, Dinaric Alps, Apennines, Balkan and Carpathian Mountains, Cambrian Mountains and Pennines in UK; over these areas the coarse resolution of ETo may be not appropriate and also small differences in the geolocation of the two datasets may cause large differences.

The use of ET/ETo further highlighted that over some areas a very small dynamic was observed; we therefore decided to mask out all the areas where the maximum range of variability of ET/ETo was smaller than 0.1 (white areas in Fig. 6), since a correlation analysis on such small range is not significant considering the models' accuracy. It is interesting to notice how these white spots are generally surrounded by pixels with low or negative *r* (e.g., Denmark, Germany, England), suggesting that these areas are characterized by a limited variability as well. Overall, the areas commonly characterized by severe water deficit conditions (mainly the Mediterranean) keep the *r* values high even for ET/ETo.

Some of the differences observed in the correlation maps can be explained by the analysis of the results obtained in the sites covered by in-situ measurements, as discussed in the next section.

4.2 Evaluation against in-situ measurements

The daily ET values collected in the 14 Fluxnet sites were used to integrate the previous intercomparison between the two models. Even if the in-situ observations are collected over footprints that are usually smaller than the simulation pixel size (5-km), they may provide useful information on the global accuracy of the two land-surface models.

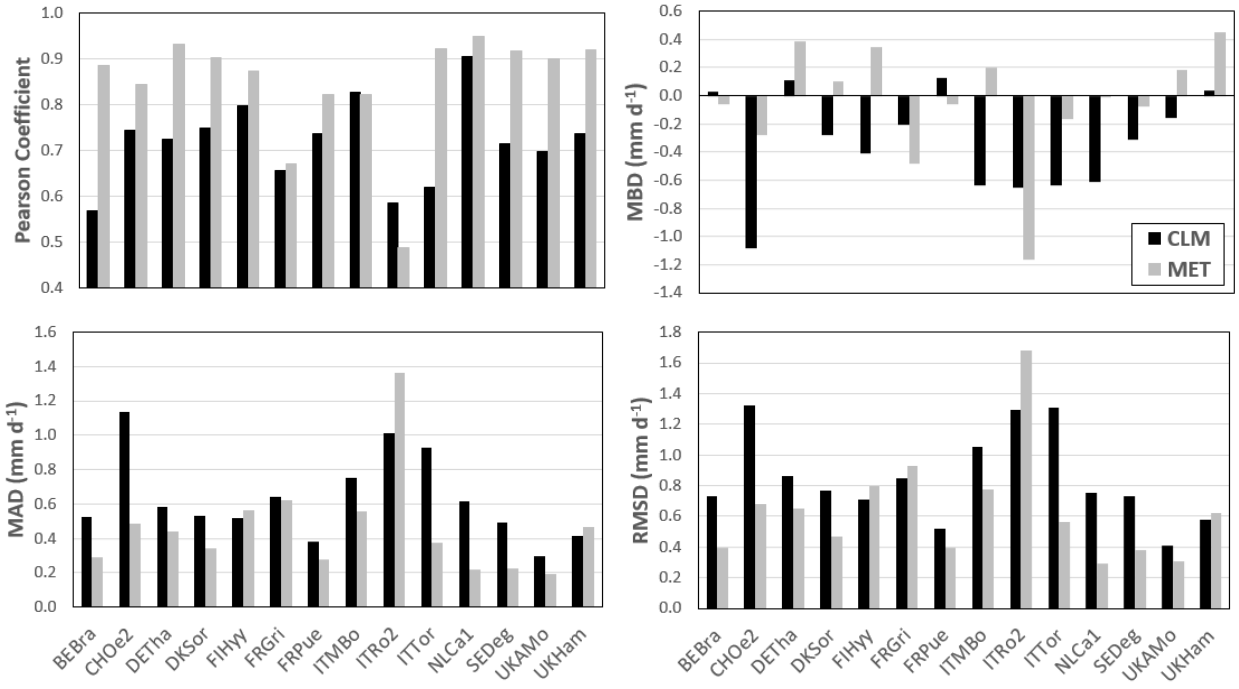

Figure 7. Barplots representing the statistical metrics computed for each Fluxnet site for CLM (black bars) and MET (grey bars) models. The upper-left panel shows the Pearson coefficient (*r*), the upper-right panel depicts the Mean Bias Difference (MBD), the lower-left panel reports the Mean Absolute Difference (MAD) and the lower-right panel reports the Root Mean Square Difference (RMSD).

The analysis was focused on the computation of both agreement and accuracy statistical metrics; in particular, the Pearson correlation coefficient was computed to quantify the agreement, whereas the Mean Absolute Difference (MAD), the Root Mean Square Difference (RMSD) and the Mean Bias Difference (MBD) were calculated to quantify random (MAD and RMSD) and systematic (MBE) errors. These metrics are reported as barplots in Fig. 7.

The Pearson coefficient values (Fig. 7, upper-left panel) are generally higher than 0.5 with maximum values around 0.9 for several sites. Overall the values obtained for MET are higher than the ones for CLM with the only exception for ITRo2 site; however, over this site both models have the worst performance. The indices of accuracy MAD (Fig. 7, lower-left panel) and RMSD (Fig. 7, lower-right panel) show that most of the sites have MAD < 0.6 and RMSD < 0.8 mm d^{-1}, with significantly higher errors for ITRo2 only for MET and for ITRo2, ITTor and CHOe2 for CLM.

The MBD data reported in Fig. 7 (upper-right panel) show that most of the errors observed in MAD and RMSD are due to systematic biases, see as examples the clear underestimation of CLM over CHOe2 and of MET over ITRo2. Overall, MET seems characterized by smaller biases of both signs, whereas CLM biases are mainly constituted by systematic underestimations.

The ITTor and CHOe2 sites are close to the Alps (one of the mountainous areas where most of the low correlation values for ET/ETo occur), whereas FRGri is located in the area where the ET maps have a low correlation (see Fig. 6); for this reason, in Fig. 8 the dynamic of both monthly ET (left panels) and ET/ETo (right panels) are reported for CHOe2 (upper line) and FRGri (lower line).

The dynamic of ET simulated by the two models for CHOe2 site (Fig. 8, upper-left panel) highlights their great similarity (r = 0.91), as well as the similarity with ETo dynamic; this results in two rather flat ET/ETo lines (Fig. 8, upper-right panel), despite the quite different values (about 0.85 and 0.6 for MET and CLM, respectively). This small dynamic is the main cause of the low (negative) correlation observed for ET/ETo (r = −0.20). Similar results were also observed for ITTor and UKAmo (not shown). For CHOe2 it was observed a systematic negative bias for CLM (see Fig. 7), hence in this case MET seems more in agreement with the observations. This behavior may be explained by the added value of remote sensing radiation forcing on such complex areas compared to interpolated meteorological maps.

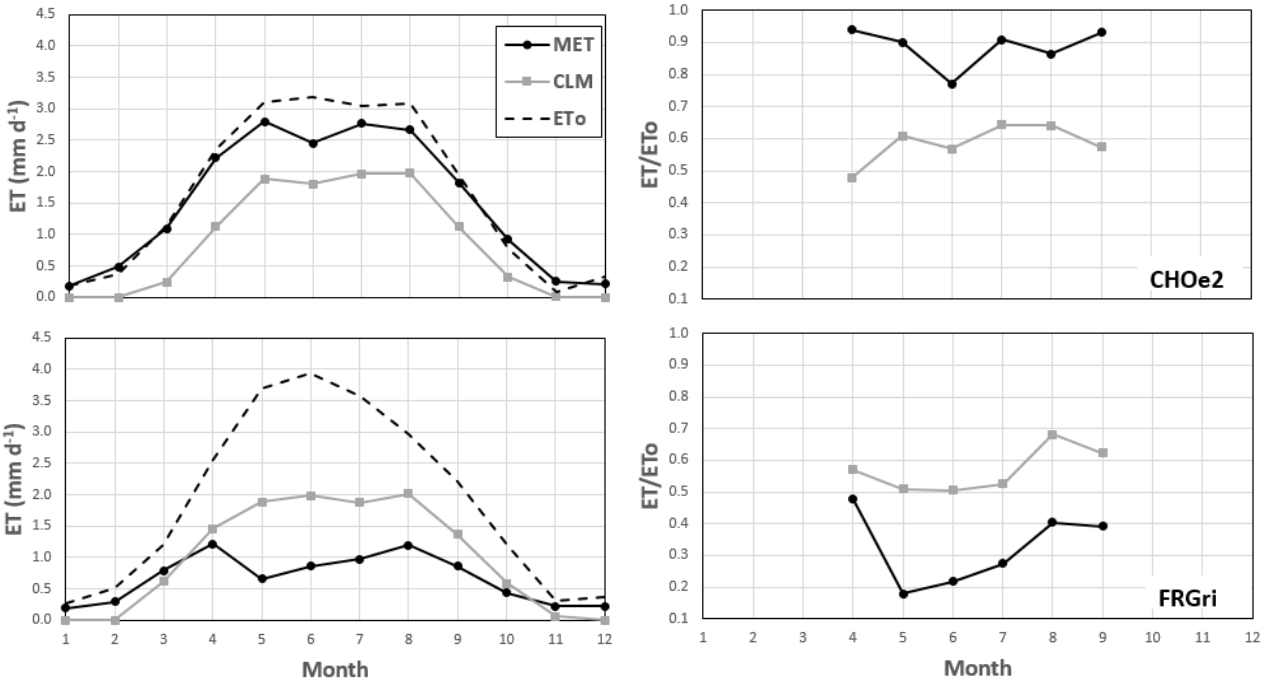

Figure 8. Temporal dynamic of ET (left panels) and ET/ETo (right panels) simulated by MET (grey line) and CLM (black line) over CHOe2 (upper line) and FRGri (lower line). The dashed line in the ET plots represents the reference evapotranspiration, ETo, derived from the FOODSEC dataset.

Table 2. All-site average statistical indices obtained for CLM and MET models against in-situ observations collected in 14 Fluxnet sites.

INDEX	CLM	MET
r	0.70	0.83
MAD (mm d^{-1})	0.62	0.48
RMSD (mm d^{-1})	0.85	0.67
MBD (mm d^{-1})	-0.25	-0.07
|MBD|* (mm d^{-1})	0.31	0.32

* The values |MBD| were obtained as weighted average of the absolute values of MBD for each station.

On the other side, the ET dynamic for FRGri (Fig. 8, lower-left panel) highlight a large leap in the ET values from April to May simulated by MET, whereas CLM shows a sort of plateau from May to July. The differences observed in these two months are the main cause of the low (negative) correlation observed in Fig. 6 for this site (r = -0.12); however, the plot of ET/ETo shows a good correspondence in the dynamic of this quantity simulated by the two models, with CLM characterized by a smaller bias (see Fig. 7). It seems that MET overestimates the effect of rainfall shortage at the start of the drought period, whereas CLM better capture the reduction of ET from the potential condition likely due to a better modelling of soil moisture dynamics.

The data in Table 2 summarize the statistical indices computed for the two models against in-situ data, reporting the all-site average values. These values were computed as weighting average by taking into account the actual sample size for each site. In the case of MBD two different average values were computed, the first by simple averaging the actual values of MBD and the second, |MBD|, computed as average of the absolute values.

The average data reported in Table 2 clearly synthetize a better agreement of MET data with the observations compared to CLM; the MAD for MET (0.48 mm d^{-1}) can be considered comparable with the expected accuracy for such product and *r* (0.83) highlights a good capability to reproduce the observed ET dynamic. The errors obtained for CLM, even if larger than the ones obtained for MET, are still acceptable for such large area applications. The |MBD| values show that the two models have similar absolute value average biases, however CLM systematically underestimates the observations (-0.25 mm d^{-1}) whereas MET is close to 0. Given that no closure was forced on the observed data, it is expected that "real" ET should be (eventually) greater than the observed one; this consideration further corroborates the better agreement of MET data with observation in terms of ET magnitude compared to CLM.

5. SUMMARY AND CONCLUSIONS

In this study a preliminary comparison between two different datasets of actual evapotranspiration, ET, was performed. The first is represented by the ET maps modelled through the CLM model, which represents one of the most sophisticate land-surface model currently developed, whereas the second is derived from the MET products developed by LSA SAF using extensively Meteosat remote sensing data.

The comparison, mainly focused on the data collected during 2011, highlighted several analogies between the two ET outputs, especially in terms of spatial distribution of the ET maps and temporal correlation of the two products. CLM and MET maps clearly show systematic differences (bias) along the whole year, but mainly focused on summer months; during this period CLM tends to underestimate MET, and this is also confirmed by the comparison with in-situ data recorded by 14 Fluxnet stations. The analysis against in-situ data also highlights that MET is generally characterized by lower errors and higher correlation compared to CLM.

Most of the difference between the two models can be observed over impervious (mountainous) areas, as clearly heighted by the correlation analysis performed on normalized (through ET_o) maps. These results somehow confirm the

need of specific adjustments of the models over such complex terrains; indeed, both models may be considered inadequate in reproducing the complex dynamic of ET over impervious area, due to the simplistic approach adopted in accounting for complex morphology. Other differences between the two models (e.g., over England, Denmark and Northeast Germany) were caused by the small dynamic of ET/ETo, suggesting the need to extend the analysis to a longer timespam.

Overall, the correlation observed between the two models, as well as the relative good accuracy against in-situ data, indicate the potentiality of using either product as reliable representation of ET status over the European domain. MET approach slightly outperform CLM, but it may take further advantage from a more sophisticate modelling of soil water content, somehow similar to CLM. On the other hand, CLM estimates could be improved by an integration of the detailed information available at LSA SAF on radiation forcing into the modelling framework. Additionally, due to the full modelling of water and energy budget, CLM may be further integrated with other LSA SAF products, as land surface temperature maps.

Lack of long term MET records does not allow a full analysis of ET anomalies, which is the standard way to detect drought events. On one side, standardization procedures involved in anomalies computation should minimized the problems related to the bias observed between the two products; however, the orderliness of these biases should be confirmed by an analysis on a longer timespan. The limited temporal coverage of satellite data currently represents the main drawback on the use of MET into an operational drought monitoring system.

ACKNOWLEDGMENTS

The authors would like to thank the EC-JRC Floods group for providing meteorological forcing for CLM, and LSA-SAF colleagues for making freely available the MET product, as well as all the researchers that are part of Fluxnet for making their measurements publicly available.

REFERENCES

[1] de Roo, A., Wesseling, C., van Deusen, W., "Physically based river basin modelling within a GIS: The LISFLOOD model," Hydrol. Process. 14, 1981-1992 (2000).
[2] Chen, J. M., Chen, X., Ju, W., Geng, X., "Distributed hydrological model for mapping evapotranspiration using remote sensing inputs," J. Hydrol. 305(1-4), 15-39 (2005).
[3] Norman, J. M, Kustas, W. P, Humes, K. S. "A two-source approach for estimating soil and vegetation energy fluxes in observations of directional radiometric surface temperature," Agric. For. Meteorol. 77, 263-293 (1995).
[4] Bastiaanssen W. G. M., Menenti, M., Feddes, R.A., Holtslag, A. A. M., "Remote sensing surface energy balance algorithm for land (SEBAL): 1. Formulation," J. Hydrol. 212-213(1-4), 198-212 (1998).
[5] Pitman, A. J., "Te evolution of, and revolution in, land surface schemes designed for climate models," Int. J. Climatol. 23, 479-510, doi:10.1002/joc.893 (2003).
[6] Oleson, K. W. and co-authors, "Technical Description of version 4.0 of the Community Land Model (CLM)," NCAR/TN-478+STR, available at: www.cesm.ucar.edu/models/cesm1.0/clm/CLM4_tech_Note.pdf (2010).
[7] LSA-SAF, "Meteosat Second Generation Evapotranspiration (MET) Product and Daily MET (DMET) Product. Algorithm Theoretical basis Document," available at: http://landsaf.meteo.pt/GetDocument.do?id=287 (2010).
[8] Ghilain N., Arboleda A., Gellens-Meulenberghs F., "Evapotranspiration modelling at large scale using near-real time MSG SEVIRI derived data," Hydrol. Earth Syst. Sci. 15, 771-786, doi:10.5194/hess-15-771-2011 (2011).
[9] van den Hurk, B. J. J. M., Viterbo, P., Beljaars, A. C. M., Betts, A. K., "Offline validation of the ERA-40 surface scheme," ECMWF Tech. Memo. No. 295 (2000).
[10] Collatz, G. J., Ball, J. T., Grivet, C., Berry, J. A., "Physiological and environmental regulation of stomatal conductance, photosynthesis, and transpiration: A model that includes a laminar boundary layer," Agric. For. Meteor. 54, 107-136 (1991).
[11] Collatz, G. J., Ribas-Carbo, M., Berry, J. A., "Coupled photosynthesis-stomatal conductance model for leaves of C4 plants," Aust. J. Plant Physiol. 19, 519-538 (1992).

[12] Sellers, P. J., Randall, D. A., Collatz, G. J., Berry, J. A., Field, C. B., Dazlich, D. A., Zhang, C., Collelo, G. D., Bounoua, L., "A revised land surface parameterization (SiB2) for atmospheric GCMs. Part I: Model formulation," J. Climate 9, 676-705 (1996).
[13] Farquhar, G. D., von Caemmerer, S., and Berry, J. A., "A biochemical model of photosynthetic CO_2 assimilation in leaves of C3 species," Planta 149, 78-90 (1980).
[14] Chehbouni, A., Lo Seen, D., Njoku, E. G., Monteny, B., "A coupled hydrological and ecological modelling approach to examine the relationship between radiative and aerodynamic surface temperature over sparsely vegetated surfaces," Remote Sens. Environ. 58, 177-186 (1996).
[15] Jarvis, P. G., "The interpretation of the variations in leaf water potential and stomatal conductance found in canopies in the field," Ph. Tran. Roy. Soc. Lon. B 273, 593-610 (1976).
[16] Lawrence, P. J., Chase, T. N., "Representing a new MODIS consistent land surface in the Community Land Model (CLM 3.0)," J. Geophys. Res. 112, G01023, doi:101029/2006JG000168 (2007).
[17] Ke, Y., Leung, L. R., Huang, M., Coleman, A. M., Li, H., Wigmosta, M. S., "Development of high resolution land surface parameters for the Community Land Model," Geosci. Model Dev. 5, 1341-1362 (2012).
[18] Masson, V., Champeaux, J. -L., Meriguet, C., Lacaze, R., "A global database of land surface parameters at 1-km resolution in meteorological and climate models," J. Climate 16(9), 1261-1282 (2003).
[19] Lawrence, P. J., Chase, T. N., "Representing a MODIS consistent land surface in the Community Land Model (CLM 3.0): Part 1. Generating MODIS consistent land surface parameters, Coop. Inst. For Res. In Environm. Sci., Univ. of Colorado, Boulder, CO (2006).
[20] Lawrence, D. M., Slater, A. G., "Incorporating organic soil into a global climate model," Clim. Dyn. 30, 145-160 (2008).
[21] LSA-SAF, "Meteosat Second Generation Land Surface Albedo Product. Algorithm Theoretical basis Document," available at: http://landsaf.meteo.pt/GetDocument.do?id=468 (2012).
[22] Qian, T., Dai, A., Trenberth, K. E., Oleson, K. W., "Simulation of global land surface conditions from 1948-2004. Part I: Forcing data and evaluation," J. Hydrometeorol. 7, 953-975 (2006).
[23] Ntegeka, V., Salamon, P., Gomes, G., Sint, H., Lorini, V., Zambrano-Bigiarini, M., Thielen, J., "EFAS-Meteo: A European daily high-resolution gridded meteorological data set for 1990-2011," Tech. rep., EC-JRC, Luxembourg: Publications Office of the European Union (2013).
[24] LSA-SAF, "Meteosat Second Generation Downward Surface Short-wave Flux Product. Algorithm Theoretical basis Document," available at: http://landsaf.meteo.pt/GetDocument.do?id=469 (2012).
[25] LSA-SAF, "Meteosat Second Generation Downward Surface Long-wave Flux Product. Algorithm Theoretical basis Document," available at: http://landsaf.meteo.pt/GetDocument.do?id=298 (2009).
[26] Twine, T. E., Kustas, W. P., Norman, J. M., Cook, D. R., Houser, P. R., Meyers, T. P., Prueger, J. H., Starks, P. J., Wesely, M. L., "Correcting eddy-covariance flux underestimates over a grassland," Agr. Forest Meteorol. 103, 279-300 (2000).
[27] Wilson, K., Goldstein, A., Falge, E., Aubinet, M., Baldocchi, D. D., Berbigier, P., Bernhofer, C., Ceulemans, R., Dolman, H., Field, C., Grelle, A., Ibrom, A., Law, B.E., Kowalski, A., Meyers, T., Moncrieff, J., Monson, R., Oechel, W., Tenhunen, J., Valentini, R., Verma, S., "Energy balance closure at FLUXNET sites," Agr. Forest Meteorol. 113, 223-243 (2002).
[28] Albergel, C., Dorigo, W., Reichle, R. H., Balsamo, G., de Rosnay, P., Muñoz-Sabater, J., Isaksen, L., de Jeu, R., Wagner, W., "Skill and Global Trend Analysis of Soil Moisture from Reanalyses and Microwave Remote Sensing," J. Hydrometeorol. 14, 1259-1277 (2013).
[29] European Drought Observatory, "Drought News in Europe: Situation in May 2011, available at: http://edo.jrc.ec.europa.eu/documents/news/EDODroughtNews201105.pdf, last access: July 2014.